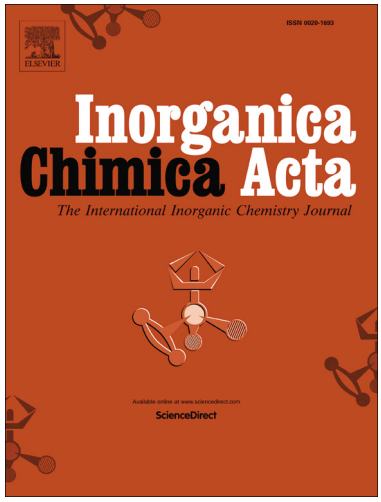

Research paper

Synthesis, structure, and photoluminescence properties of lanthanide based metal organic frameworks and a cadmium coordination polymer derived from 2,2'-diamino-*trans* 4,4'-stilbenedicarboxylate

Saki T. Golafale, Conrad W. Ingram, John Bacsa, Alexander Steiner, Kyril M. Solntsev

PII: S0020-1693(17)31501-3
DOI: https://doi.org/10.1016/j.ica.2018.04.005
Reference: ICA 18196

To appear in: *Inorganica Chimica Acta*

Received Date: 28 September 2017
Revised Date: 1 April 2018
Accepted Date: 4 April 2018

Please cite this article as: S.T. Golafale, C.W. Ingram, J. Bacsa, A. Steiner, K.M. Solntsev, Synthesis, structure, and photoluminescence properties of lanthanide based metal organic frameworks and a cadmium coordination polymer derived from 2,2'-diamino-*trans* 4,4'-stilbenedicarboxylate, *Inorganica Chimica Acta* (2018), doi: https://doi.org/10.1016/j.ica.2018.04.005

Synthesis, structure, and photoluminescence properties of lanthanide based metal organic frameworks and a cadmium coordination polymer derived from 2,2'-diamino-*trans* 4,4'-stilbenedicarboxylate

Saki T. Golafale[a], Conrad W. Ingram[a]*, John Bacsa[b], Alexander Steiner [c] and Kyril M. Solntsev[d]

[a]*Chemistry Department, Clark Atlanta University, Atlanta, GA, 30314, USA*
[b]*X-ray Crystallography Center, Emory University, Atlanta, GA, 30322, USA*
[c]*Department of Chemistry, University of Liverpool, Liverpool L69 7ZD, UK*
[d]*School of Chemistry and Biochemistry, Georgia Institute of Technology, Atlanta, GA 30332, USA.*

**Correspondence email: cingram@cau.edu*

Abstract

Two isostructural lanthanide-based metal - organic frameworks, $\{[Ln(C_{16}H_{12}N_2O_4)(CHO_2)(OH_2)\cdot 2(C_5H_{11}NO)]\}_n$, Ln =Yb (**1**) and Tm (**2**), and a cadmium(II) coordination polymer, $\{[Cd_2(C_{16}H_{12}N_2O_4)(NO_3)\cdot 4(C_3H_7NO)]\}_n$, were synthesized by the combination of the respective metal nitrate and 2,2'-diamino-*trans* 4,4'-stilbenedicarboxylate ($C_{16}H_{12}N_2O_4$) under solvothermal conditions [$C_5H_{11}NO$ = diethylformamide and C_3H_7NO = dimethylformamide]. Their structures were determined by X-ray single crystal analysis, X-ray powder diffraction, Fourier transformed infrared spectroscopy, elemental analysis, thermogravimetric analysis and solid state photoluminescence spectroscopy. Both lanthanide structures are infinite three-dimensional non-penetrating networks with extremely large diamond shape accessible channels of cross-sectional dimensions [30 Å x 12 Å] and with the amino-functional groups projecting into the channels. The cadmium-based structure is a one-dimensional coordination polymer with both the carboxylate and the amino groups coordinating the cadmium atoms, which resulted in a large increase in the rigidity of the ligand. Ligand-based fluorescence was exhibited by all three networks, with the cadmium based structure showing the highest intensity and longest fluorescence radiative lifetime.

1. Introduction

Metal-organic frameworks (MOFs) and coordination polymers (CP) offer great promise for applications in important areas, such as optical sensing, adsorption, and catalysis, among others. [1 - 5] One factor that is often limiting the porosity of open frameworks is interpenetration. *Trans*-stilbene and its amino-substituted derivatives represent a class of

organic molecules that are of great significance as components of linker units in MOF and CP structures because they can be used to construct open, non-interpenetrating frameworks. Such open framework architectures generated by these molecules can be exploited for adsorption, while their highly luminescent characteristics arising from their π-conjugated chromophores can be exploited for optical sensing. In fact, *trans*-stilbenoid molecules are used in many solid-state scintillating devices because of their radioluminescence properties.[6,7] In the case of amino-substituted *trans*-stilbenes, the amino groups can alter the luminescence behaviour of the parent stilbene. Diamino-stilbenes are reported to have longer excited state lifetimes than *trans*-stilbene, due to the delocalization of the lone pair of electrons on the amino group. [8,9] Consequently, substituted amino-stilbenoid derivatives, such as diamino-stilbenedicarboxylic acid, are the active materials in a variety of optoelectronic devices, such as organic light emitting diodes and solar cells. [10-19] As the organic linkers in MOF and CP structures, the amino-stilbenoid derivatives may not only alter the photophysics of the materials, but the amino groups can also function as sites for adsorption, chemical sensing and Lewis base catalysis .[20-26] However, when exposed to photo- or ionizing radiation, stilbenes can undergo *trans-cis* isomerization, leading to energy loss through non-radiative relaxation that can significantly reduce their luminescence efficiency and quantum yield.[27,28] Inhibition of motion around the central ethylene bond, by locking the molecule in *trans*-geometry, is considered as an effective solution to suppress *trans-cis* isomerization.

Recently, we demonstrated that the combination of *trans* 4,4'-stilbene dicarboxylic acid, with the lanthanide ions, Tm^{3+} and Er^{3+} generated non-interpenetrating ultra large pore structures, with the stilbene units anchored by the metal ions through the carboxylate groups.[29] The anchoring not only suppressed *trans-cis* isomerization activity, but also, the separation between the units reduced the inter-chromophore coupling which would otherwise be extensive in the powdered bulk solid of the pure ligand, on the exposure to ionizing and UV radiation. The resulting structures showed increased radio- and photo-luminescence lifetimes over that of the organic molecule in its solid form. Similar luminescence behavior was previously reported for Zn-based MOFs containing the *trans* 4,4'-stilbene moiety. [30,31]

Numerous MOFs and CPs have been reported from the combination of the *trans* 4,4'-stilbene moiety with a wide range of metals ions, among which are Cd, [32-37] Co,[38-40] Cu[41], Mn,[42] Pb, [43,44] Zn,[45-49] Zr[50],[51], lanthanide ions[52-54] and mixed transition metal ions, [31] but these are mostly interpenetrating networks. Following the success of creating mesoporous

frameworks with *trans*-stilbene dicarboxylate, we sought to explore the use of the diamino- substituted stilbene ligand, 2,2-diamino-4,4'-stilbenedicarboxylic acid, H_2L, for the synthesis of MOFs and CPs. The lanthanide metals were chosen based on their large size and their high propensity for high coordination numbers, which can promote 3-D connectivity, whereas cadmium was selected as the transition metal ion based on its d^{10} electron configuration.

We herein report two isostructural lanthanide metal-based MOFs $\{[Ln(C_{16}H_{12}N_2O_4)(CHO_2)(OH_2).2(C_5H_{11}NO)]\}_n$, Ln =Yb (**1**) and Tm (**2**)], and one cadmium-based CP,$\{[Cd_2(C_{16}H_{12}N_2O_4)(NO_3)\cdot 4(C_3H_7NO)]\}_n$, $C_{16}H_{12}N_2O_4$ = 2,2'-diamino-*trans* 4,4'-stilbenedicarboxylate, L], that were synthesized from the combination of H_2L and the nitrate salts of the respective metals, under solvothermal conditions. The lanthanide metal based structure (**1** and **2**) crystalizes as a non-interpenetrating 3-D coordination network, and features large diamond shape accessible channels of dimensions, 30 Å x 12 Å, which are occupied by diethylformamide that was used as solvent in the synthesis. The solvent molecules are hydrogen bonded to the amino groups of the framework, which project into the channels. The cadmium based structure, **3**, is a one-dimensional coordination polymer. The structures show ligand-based fluorescence with spectral characteristics, radiative intensities and lifetimes that appear to correlate with the orientation and coordination behavior of the ligands. The cadmium based structure, shows fluorescence of strongest intensity and longest florescence lifetime among the three compounds.

2. Experimental

Synthesis

All solvents and metal salts were purchased from Aldrich and used as received. Structures **1** and **2** were synthesized by mixing lanthanide (III) nitrate pentahydrate (**1**. $Yb(NO_3)_3\cdot 5H_2O$ = 44.6 mg, 0.10 mmol, and **2**. $Tm(NO_3)_3\cdot 5H_2O$ = 44.7 mg, 0.10 mmol) and H_2L (4.00 mg, 0.01 mmol) with N,N-diethylformamide (DEF, 1 mL) in 20 mL scintillation vials. The sealed vials were heated under static conditions at 105° for 72 hours after which yellow needle crystals were formed. Synthesis attempts using other lanthanide ions, including, Pr^{3+}, Nd^{3+}, Sm^{3+}, Eu^{3+}, Gd^{3+}, Dy^{3+}, Tb^{3+}, Ho^{3+}, and Er^{3+} under similar experimental conditions resulted in non-crystalline powders. Structure **3** was synthesized by mixing a solution of H_2L (4.0 mg, 0.01 mmol) in DMF (1 mL) with $Cd(NO_3)_2\cdot 4H_2O$ (12.7 mg, 0.04 mmol) in a 20 mL scintillation vial and sonicating the mixture 5 minutes. The sealed

vial was heated in a programmable oven at 75 °C for 36 hours followed by 85 °C for 36 hours at heating rate of 1 °C/min heating. The crystals were recovered and washed repeatedly with fresh DMF. Transition metals such as Mn^{2+}, Fe^{3+}, Cu^{2+}, Ni^{2+}, and Zn^{2+} we attempted under similar synthesis conditions but only produced non-crystalline powders. Elemental analysis: **1**: Found, C = 44.80%, H = 5.38%, N = 9.88%; Calculated, C = 44.14%, H = 5.04%, N = 7.63%. FTIR (cm^{-1}): 1655(m), 1553 (m), 1426 (m), 1400 (m), 1286 (m), 1264(w), 1218 (w), 1111 (w), 1027 (w); **2**: Found, C = 44.86%, H = 5.14%, N = 9.39%; Calculated, C = 44.39%, H = 5.04%, N = 7.67%. FTIR (cm^{-1}): 1655(m), 1553 (m), 1426 (m), 1400 (m), 1286 (m), 1264(w), 1218 (w), 1111 (w), 1027. Differences observed between calculated and found values for C,H,N elemental analysis could be due to the presence of one non-coordinated molecule of N-nitrosodiethylamine, $(C_2H_5)_2NNO$, (a possible byroduct of DEF decomposition) per formula unit. **3**: Found: C =36.87 %, H = 4.06 %, N = 11.27 %; Calculated: C = 35.87 %, H = 4.30%, N = 11.95%. FTIR (cm^{-1}): 3328(w), 3238 (w), 3162 (w), 2917 (w), 2850 (w), 1653 (s), 1615 (w), 1519 (s), 1386 (s), 1334 (w), 1281 (s), 1109 (w), 1021 (s).

Characterization

Single crystal X-ray diffraction (SCXD) data were collected on a Bruker APEX2 diffractometer. Suitable crystals were isolated from the sample and mounted unto the instrument using Paratone Oil. The crystal was kept at 100(2) K during data collection. Measurements were made at ω scans rate of 0.5° per frame for 30.0 s for **1**, 1° per frame for 40 s for **2**, and 0.5° per frame for 15.0 s for **3,** using MoK_{α} radiation with fine-focus sealed X-ray tube, at 45 kV, 20-30 mA).

For structures **1** and **3**, the diffraction patterns were indexed and the unit cells were refined using CrysAlisPro (Agilent). Data reduction, scaling and absorption corrections were performed using CrysAlisPro (Agilent) and CrysAlisPro 1.171.39.7b.[55] Empirical absorption corrections were applied using spherical harmonics, implemented by the SCALE3 ABSPACK scaling algorithm software. For structure **2**, Olex2 was the graphical interface.[56] All three structures were solved and the space groups determined by the XT[57] structure solution program using Intrinsic Phasing and refined by Least Squares using version 2014/7 of XL.[58] All non-hydrogen atoms were refined anisotropically. Hydrogen atom positions were calculated geometrically and refined using the riding model. The total number of runs and images was based on the strategy calculation from the program APEX2.[59]

Powdered X-ray diffraction (PXRD) patterns were recorded on a Panalytical Empyrean Series II X-ray diffractometer. The X-ray source was a Cu Kα (λ = 1.5418 Å) with anode voltage of 45 kV and current of 40 mA. Diffraction patterns were recorded between the 2θ angles of 4˚- 50˚ as indicated on the PXRD patterns, with a step size of 0.026˚. Simulated PXRD patterns were obtained from SCXD data using Mercury 3.1 software from Cambridge Crystallographic Data Center. Infrared measurements were recorded on a Bruker Alpha-P FTIR spectrophotometer. The sample was introduced into the spectrophotometer using KBr as a zero background powder and measurements were acquired between 350 cm^{-1} and 4000 cm^{-1}.

Thermogravimetric analysis (TGA) was conducted on a TA Instrument Q50 thermal analyzer. Approximately 4 mg of sample was heated at a rate of 10 °C/min from ambient temperature to 900°C under air flow. Elemental analysis was performed by Atlantic Microlab, Norcross GA, USA.

Solid state photoluminescence

Room temperature solid state photoluminescence measurement was carried out on Photon Technology International fluorometer equipped with a 75 Watts Xenon Arc Lamp, excitation and emission monochromators, and a photomultiplier detector. A powdered sample of each compound was smeared between quartz slides, and excitation and emission spectra were recorded. Fluorescence lifetimes of the same samples were measured using an Edinburgh Instruments time-correlated single photon counting (TCSPC) system. In this measurement, an excitation pulse diode laser (LDH-P-C-375, 372 nm) was used as excitation light sources. The detection system consisted of a high speed MicroChannel Plate PhotoMultiplier Tube (MCP-PMT, Hamamatsu R3809U-50) and TCSPC electronics. The decay curves were fitted by the polyexponential functions after deconvolution with the instrument response function (IRF).

3. Results and Discussion

*Ln-L (**1** and **2**) structure description*

X-ray single crystal analysis shows that the lanthanide MOFs $\{[Ln(C_{16}H_{12}N_2O_4)(CHO_2)(OH_2)\cdot 2(C_5H_{11}NO)]\}_{n,}$ Ln =Yb (**1**) and Tm (**2**)] are isostructural. Structure description is therefore given for structure **2**. They exhibit monoclinic C-centered cells with very similar lattice parameters (Table 1). The structures exhibit C2/c symmetry;

the metal atoms are located on two-fold axes, while stilbene dicarboxylate groups occupy inversion centers. The lanthanide atoms form undulating rows parallel to the c-axis, and are bridged by pairs of carboxylate groups of the ligands. In return, the tetracoordinate stilbene dicarboxylate units connect these rows in *bis*-bridging mode, which results in the formation of a three-dimensional network (Figure 1a).

Both lanthanide structures are infinite 3-D non-penetrating networks. Non-penetration afforded extremely large diamond shape accessible channels of cross-sectional dimensions [30 Å x 12 Å], similar to our previously reported stilbene based structures, but with the amino-functional groups projecting into the channels. The metal center is six-coordinate. Four bonds are with one carboxylate oxygen atom from each of four diamino-stilbenedicarboxylate linker. The remaining two bonds are with the coordinated water molecule and formate ion (ESI Figure S1). The formate ion is the result of hydrolysis of DEF under the reaction conditions. Each amino group of the ligand binds a DEF molecule that resides in the void, via a hydrogen bond. We note that differences were observed between the values calculated and found for carbon, hydrogen, and nitrogen elemental content. The difference was most pronounced for nitrogen, and suggests the presence of a high nitrogen-content species. We speculate that the high nitrogen-content species is possibly N-nitrosodiethylamine, $(C_2H_5)_2NNO$, one non-coordinated occluded molecule per formula unit of the MOF structure. The formation of N-nitrosodiethylamine as a byproduct of the decomposition of DEF solvent during the synthesis of MOF-5/MOF69c has been reported by Hausdorf et al.[60]

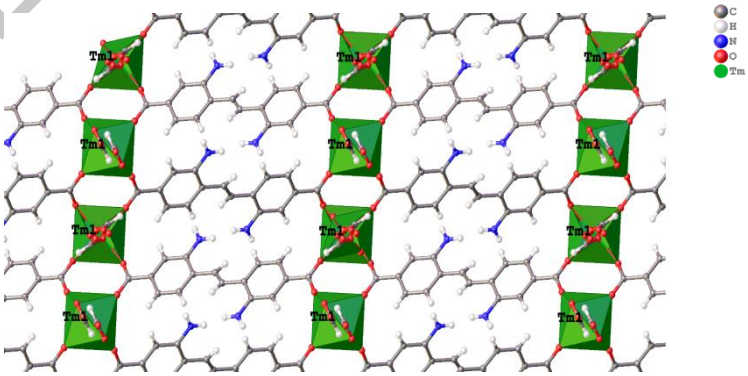

(i)

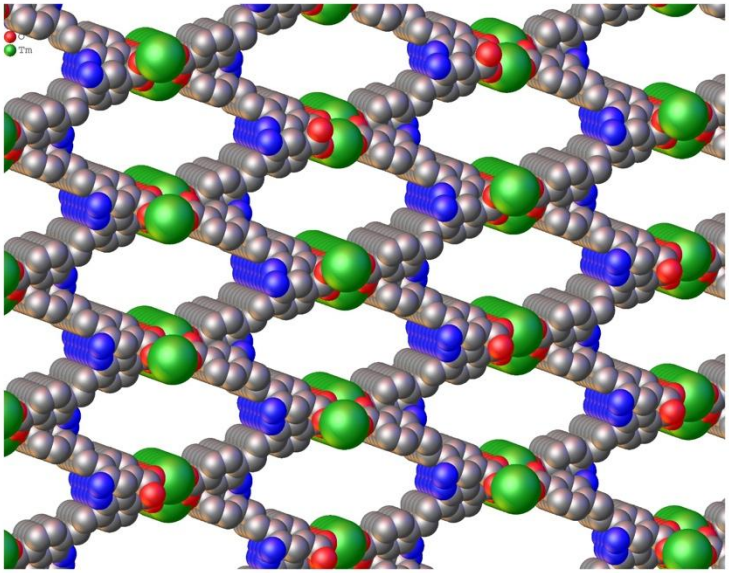

(ii)

Figure 1. (i) Partial structure of **2** showing lanthanide ions in rows parallel to the c-axis, and bridged by pairs of carboxylate groups of the ligands. (ii) Space filling model of **2** viewed along the c axis. (Tm = green, C = grey, O = red, N =blue; (hydrogen atoms and solvent molecules are omitted for clarity).

This underlying topology of the structure is that of the mineral, cooperite (PtS), with the Pt atoms representing the Tm atoms and S atoms representing the stilbenedicarboxylate moiety (Figure 1b). It is a four-coordinate and a two-nodal net with net symbol, sqc183.[61]

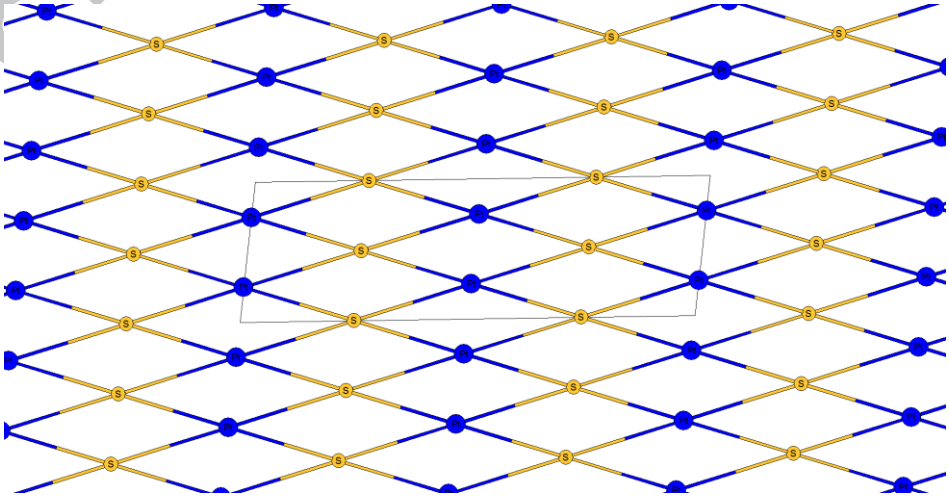

Figure 1b. Topology of **2** as a four-coordinate and a two-nodal net with net symbol, sqc183.

(Pt = blue, S = yellow)

Cd-L structure description

The crystals of $\{[Cd_2(C_{16}H_{12}N_2O_4)(NO_3)_2 \cdot 4(C_3H_7NO)]\}_n$, **3,** belong to the monoclinic system and space group $P2_1/c$. This cadmium based structure, unlike the lanthanides, is a one-dimensional coordination network. The Cd atom is seven coordinate (Figure 2a): two Cd-O bonds are with the carboxylate oxygen atoms of the coordinating ligand; two Cd-O bonds are with the coordinated DMF molecules; two Cd-O bonds are with a coordinated nitrate ion; and, the seventh is a Cd-N bond with an amine group on a neighboring linker unit. Selected bond lengths and bond angles are presented in electronic supporting information (ESI) Table S1. The Cd-O bond lengths range between 2.3097(13) Å and 2.4838(14) Å and the Cd-N bond length is 2.3877(14) Å, which are consistent with reported values.[62] Further, each $\{Cd\text{-}L\text{-}Cd\}_n$ chain is linked to two neighboring and parallel $\{Cd\text{-}L\text{-}Cd\}_n$ chains, via the N-sites of the ligand and Cd atoms in neighboring chains. This forms an infinite ladder structure (Figure 2).

Table1. Crystallographic data and structure refinement summary for **1-3**.

ID	**1**	**2**	**3**

Formula	$C_{27}H_{37}N_4O_9Yb$	$C_{27}H_{37}N_4O_9Tm$	$C_{28}H_{40}N_8O_{14}Cd_2$
$D_{calc.}$/ g cm^{-3}	1.307	1.295	1.758
μ/mm^{-1}	2.658	2.515	1.278
Formula Weight	734.04	729.93	937.48
Color	yellow	yellow	colorless
Shape	needle	needle	plate
Size/mm^3	0.18×0.16× 0.09	0.34 × 0.16 × 0.15	0.42×0.29×0.11
T/K	100(2)	100(2)	100(2)
Crystal System	monoclinic	monoclinic	monoclinic
Space Group	C2/c	C2/c	$P2_1/c$
a/Å	30.6985(16)	30.8130(7)	8.5715(2)
b/Å	12.3582(7)	12.3420(2)	20.6743(3)
c/Å	9.4977(7)	9.4989(3)	10.3011(2)
α/°	90	90.0	90
β/°	97.072(5)	96.626(2)	104.052(2)
γ/°	90	90.0	90
V/Å^3	3575.8(4)	3588.23(15)	1770.83(6)
Z	4	4	2
Z'	0.5	0	0.5
Wavelength/Å	0.710730	0.710730	0.710730
Radiation type	MoK_a	MoK_a	MoK_a
Θ_{min}/°	1.337		1.970
Θ_{max}/°	27.497		32.105
Measured Refl.	23405	24945	31969
Independent Refl.	6593	5228	5892
Reflections with I > 2(I)	5805	5228	5542
R_{int}	0.0706	0.0416	0.0328
Parameters	209	207	267
Restraints	171	171	2
Largest Peak	2.129	3.51	1.416
Deepest Hole	-1.224	-2.10	-0.431
GooF	1.131	1.093	1.072
wR_2 (all data)	0.2653	0.1943	0.0728
wR_2	0.2499	0.1855	0.0715
R_1 (all data)	0.1073	0.0790	0.0305
R_1	0.0953	0.078	0.0283

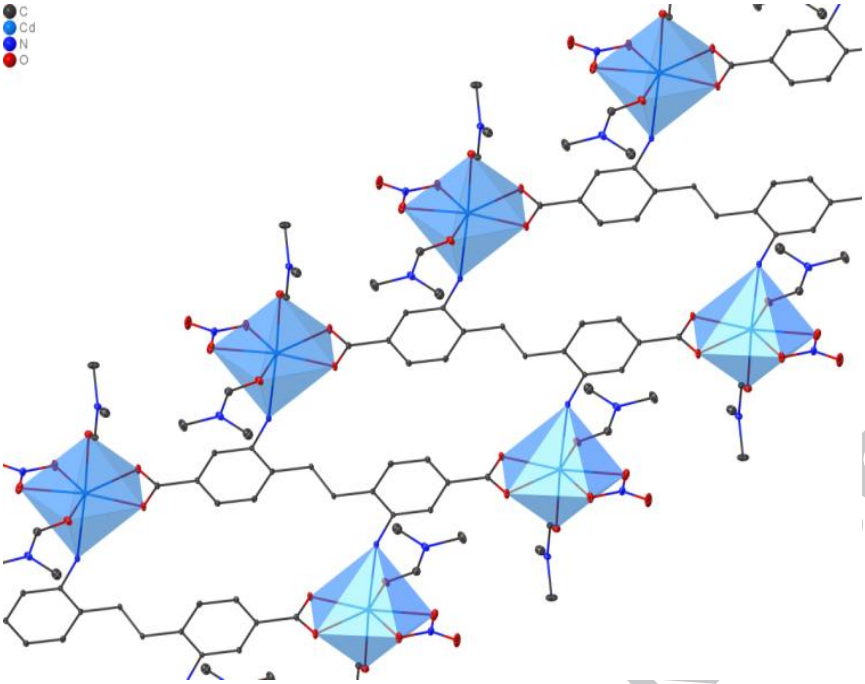

Figure 2a. The one-dimensional ladder structure of **3**.

The underlying topology of this one-dimensional chain structure is a 2,4-coordinate net with point symbol $\{4^2\}\{4\}2$ (the point symbol for the net with loops is $\{2^2\}\{2\}2$).[61] The Cd atoms have the face symbol {4} indicating that it is a vertex of 4-ring and that there is only one ring here (Figure 2b). The nodes of the bridging ligands are represented by Sc atoms and have the have the face symbol $\{4^2\}$ indicating they are vertices of two 4-rings. The topology of the underlying net is **2,4C4** in the standard representation of valence-bonded MOFs.

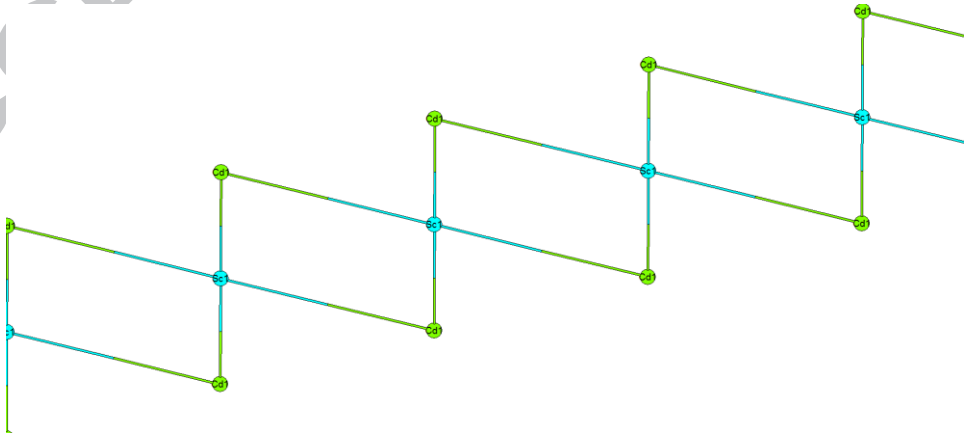

Figure 2b. The underlying topology of the one-dimensional chain structure of **3** as a 2,4-coordinate net with point symbol $\{4^2\}\{4\}$.

PXRD and thermal analysis

The X-ray powder diffraction patterns of structures **1**, **2** and **3** closely match their simulated patterns (ESI Figures S2 and S3). This further supports single crystal X-ray analysis, thus confirming that compounds **1** and **2** are isostructural. In addition, the close matching of the powder diffraction peaks to those of the simulated patterns and the absence of additional peaks indicate that each structure crystallized as a pure phase. The structures are stable in air and in chloroform. However extended evacuation at ambient or elevated temperatures or exposure to solvents including water, methanol, and methylene chloride in an effort to remove occluded DEF molecules, resulted in substantial irreversible structural changes with partial loss of crystallinity (as determined by powdered XRD, not shown).

FTIR spectra

The Fourier transformed infrared (FTIR) spectra of **1**, **2**, **3** and H_2L, were compared. (ESI Figure S4.) Peaks at 3458 cm^{-1} and 3379 cm^{-1} in the free ligand are assigned to N-H stretching. These peaks disappear in **1** and **2,** most likely due to H-bonding with coordinated DEF. These peaks are redshifted to 3238 cm^{-1} and 3162 cm^{-1} in compound **3**; the redshift is speculated to be caused by the coordination of the N atoms to the metal atoms which weakens the bond. Whereas as the C=O stretching vibration peaks are observed at 1673 cm^{-1}, 1628 cm^{-1} and 1606 cm^{-1} for H_2L, the peaks seem to merge at 1657 cm^{-1} for **1** and **2** and at 1653 cm^{-1} for **3** due to deprotonation of the ligand in the structures and the formation of partial of C=O-metal coordination. The C-N stretching vibration is observed at 1255 cm^{-1} and 1294 cm^{-1} for H_2L while they are redshifted to 1286 cm^{-1} for both **1** and **2** and to 1281 cm^{-1} for **3**. Peaks observed at 1120 and 1142 cm^{-1} for H_2L are also assigned to C-O stretching, and are observed at 1112 cm^{-1} and 1027 cm^{-1} for **1** and **2**.

Thermal Analysis

The thermal behavior of structures **1-3** was investigated by TGA. The TGA curves of compounds **1** and **2** are similar, and show three weight loss events (ESI Figure S5). Weight loss up to 180 °C amounting to 25 wt. % is attributed to the loss of non-coordinated DEF molecules. Further weight loss between 312 °C and 380 °C that amounts to approximatly10 wt. % is attributed to loss of coordinated formate ion and H_2O. Weight loss between 398 °C

and 550 °C and amounting to 26 % is attributed to decomposition of the diamino-*trans* – stilbenedicarboxylate organic linker. The residual weight of 25 wt. % is attributed to the metal oxide. The TGA curve of **3** shows three main weight loss events. The first occurs between 145 °C and 190 °C, and amounts to approximately 18 wt. %. This is attributed to decomposition of coordinated DMF. The second event between 200 °C and 230 °C that constitutes about 12 wt. % is attributed to loss of coordinated NO_3^- species. Weight loss between 250 °C and 450 °C that constituting approximately 40 wt. % is attributed to the decomposition of the organic linker. The residual weight of 28 wt. % is attributed to the metal oxide.

Photoluminescence

The linker units are located in similar structural environment in **1** and **2**, but in a different environment in **3,** thus allowing for a comparison of their photoluminescence properties. Like solid H_2L, upon illumination with UV radiation of wavelength of 370 nm, **1** and **2** show emissions of comparable brightness and moderate to the eye, whereas the emission from **3** was significantly brighter. The combined excitation and emission spectra of chloroform soaked solid samples of **1**, **2, 3** and H_2L are presented in Figure 3. The spectra are in general, broad and featureless, and show $\lambda_{max\ ex}$ values that correspond with the $\lambda_{max\ abs}$ reported for aminostilbenes and diaminostilbenes[63,64]. The emission spectral profile for **1** and **2** are similar to that observed for H_2L, showing one broad featureless band, whereas the emission spectrum of **3** shows partially resolved vibronic peaks. The differences observed in the electronic spectra for **1, 2** and **3** likely originate from several factors, such as the local coordination environment of the ligand and the steric proximity of ligand units to each other. Nevertheless, the similarity of the spectral profiles to that of H_2L suggests that the emissions are attributed to intraligand π^*-π transitions, and not metal-to-ligand nor ligand-to-metal charge transfer.

For stilbene and its substituted derivatives, *trans-cis* photoisomerization can compete with fluorescence, following the absorption of UV radiation. Rigidifying the ligand units can restrict movement around the central ethylene bond, thereby inhibiting *trans-cis* photoisomerization, as we and others have previously shown. Also, isolation of the ligand units can lead to less inter-chromophore π–π electronic interactions, which could otherwise lead to the formation of dimer species in some instances. Both rigidifying and isolating the stilbenoid units can reduce non-radiative energy loss, leading to enhanced fluorescence

behavior of the ligand. The emission spectra of **1**, **2** and **3** are all blue shifted relative to that of powdered H_2L. The blue shift in the MOFs is attributed to both the rigidification and separation of the ligand units in these low density structures, and hence a corresponding reduction in the extent of any inter-ligand interactions among the units. This is quite similar to observations reported for lanthanide[30] and zinc based stilbene MOFs.[31,32] The blue shift is larger for **3** than for **1** or **2,** and is likely related to their structural differences. Furthermore**, 1, 2, 3** and H_2L all show significant Stokes shifts, resulting from some or all of the non-radiative energy loss related processes above, and with values estimated as follows: **1,** $\lambda_{max\ em}$ = 528 nm ($\lambda_{max\ ex}$ = 382 nm**,** Stokes shift = 146 nm); **2**, $\lambda_{max\ em}$ = 518 nm, ($\lambda_{max\ ex}$ = 345 nm, Stokes shift 173 nm); **3**, $\lambda_{max\ em}$ = 448 (shoulder, sh), 475 and 495 nm, ($\lambda_{max\ ex}$ = 351 nm sh, and 376 nm, Stokes shift = 97-120 nm), and H_2L $\lambda_{max\ em}$ = 536 nm, ($\lambda_{max\ ex}$ = 348 nm and 369 nm, Stokes shift 166 -184 nm). That the Stokes shift values for **1** and **2** are within the range observed for H_2L while the value for **3** is smaller, is again likely related to their structural differences. In **1** and **2,** the ligand units are anchored via their carboxylate groups to the metal centers, but the pendant amino functional groups remain uncoordinated. In **3** however, the amino functional groups are also engaged in interconnecting $Cd(NO_3)(DMF_2)$-L-$Cd(NO_3)(DMF_2)$ neighbouring units through $Cd\text{-}N_{(amine)}$ bonds to form a stacking arrangement. This further rigidifies the ligand within the coordination polymer structure, thereby minimizing *trans-cis* isomerization.

The nearest distance between aromatic rings of the highly separated ligand moieties in **1** and **2** is located where the ligand units converge in V - shaped arrangements during coordination to the Ln^{3+} centers, and measures ~4 Å edge-to-face. In the case of **3,** this distance measures 4.4 Å and is edge-to-edge between parallel $Cd(NO_3)(DMF_2)$-L-$Cd(NO_3)(DMF_2)$ units. Though these distances are within the range where inter-chromophore π–π interactions can be substantial[65], the non-cofacial orientation suggests that such interactions would be of intermediate strength, and is likely more sustained in structure **3** than in **1** and **2**. It is worth considering that the presence of the amino (electron donor) and carboxylate (electron acceptor) groups constitutes a donor-acceptor type ligand, which is known to promote intramolecular charge transfer (ICT) during photoisomerization. The extent to which the coordination of the Cd^{2+} ions (of d^{10} electron configuration), by the ligand's amino groups in **3** perturbs the electronic structure of the ligand and therefore its resulting fluorescence properties remains to be explored. However, recent studies have

shown that the coordination of *trans*-stilbene, to Cd^{2+} and Zn^{2+}, respectively, has little or no effect on the electronic spectra of the organic molecule. [66]

The luminescence spectral features that are characteristic of lanthanide ions were not detected in the visible region (for Tm^{3+}) and were not measured in the near infrared region (for Tm^{3+} and Yb^{3+}) which is beyond the range of our standard fluorimeter. It is speculated however, that photoemissions of these metals ions from direct excitation would be weak or non-existent due to their low molar absorption coefficient (typically lower that 10 L mol^{-1} cm^{-1}). Further, the linker, L, like most organic ligands, are poor sensitizers of these lanthanide ions, for two main reasons; (i) the low molar absorption coefficients of these metal ions, and (ii) the very small energy gaps between the first excited state and fundamental level of these metal ions are easily matched by C–H, and C=C vibrations of the ligand, all of which provide suitable non-radiative channels.[67,68] We speculate therefore that these lanthanide and Cd^{2+} ions have very little or no effect on the photoluminescence behavior of **1**,**2** and **3**.

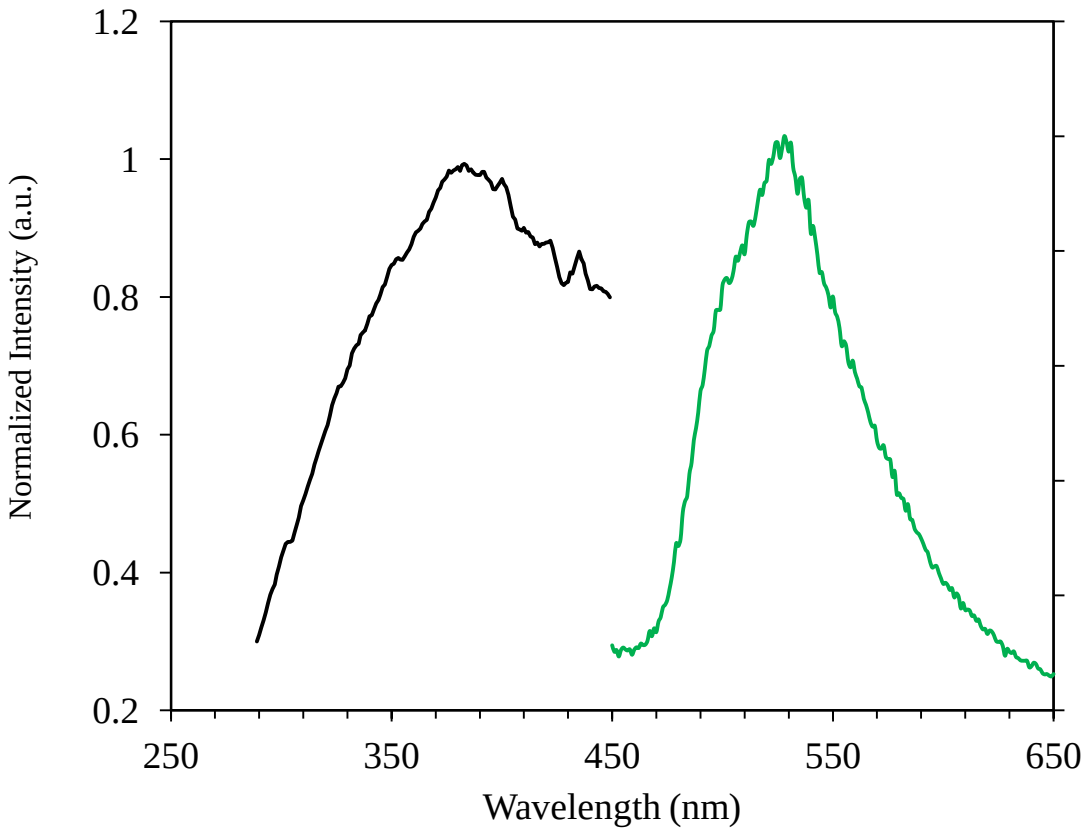

(1. Yb)

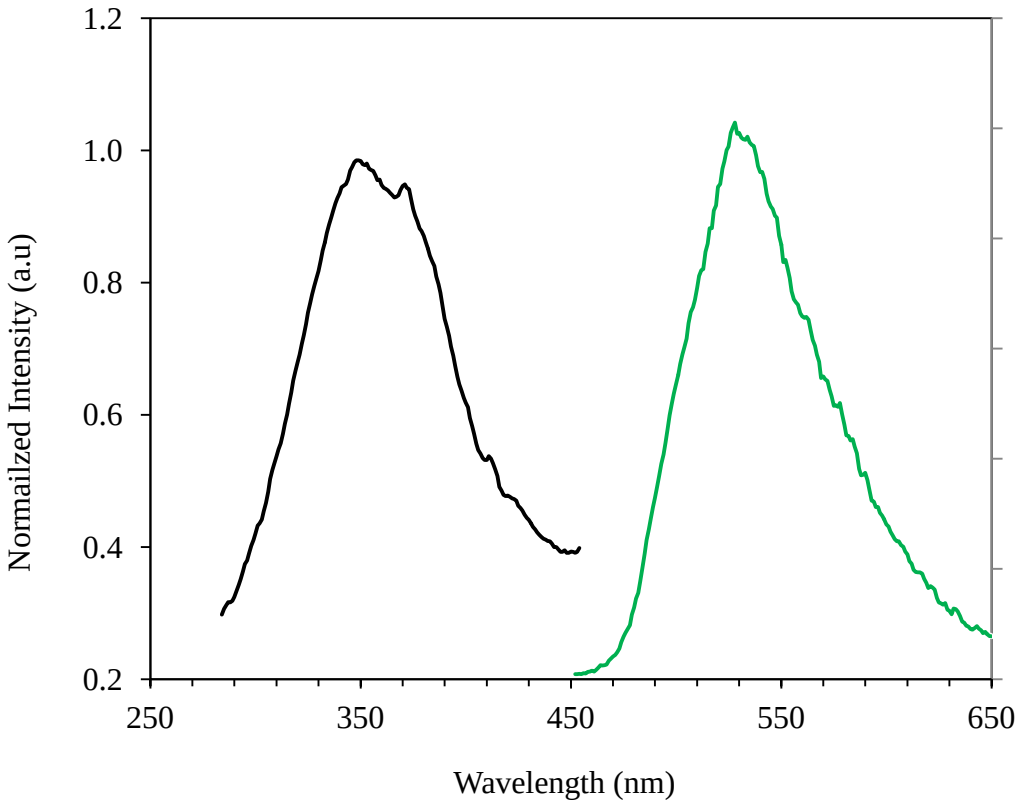

(2. Tm)

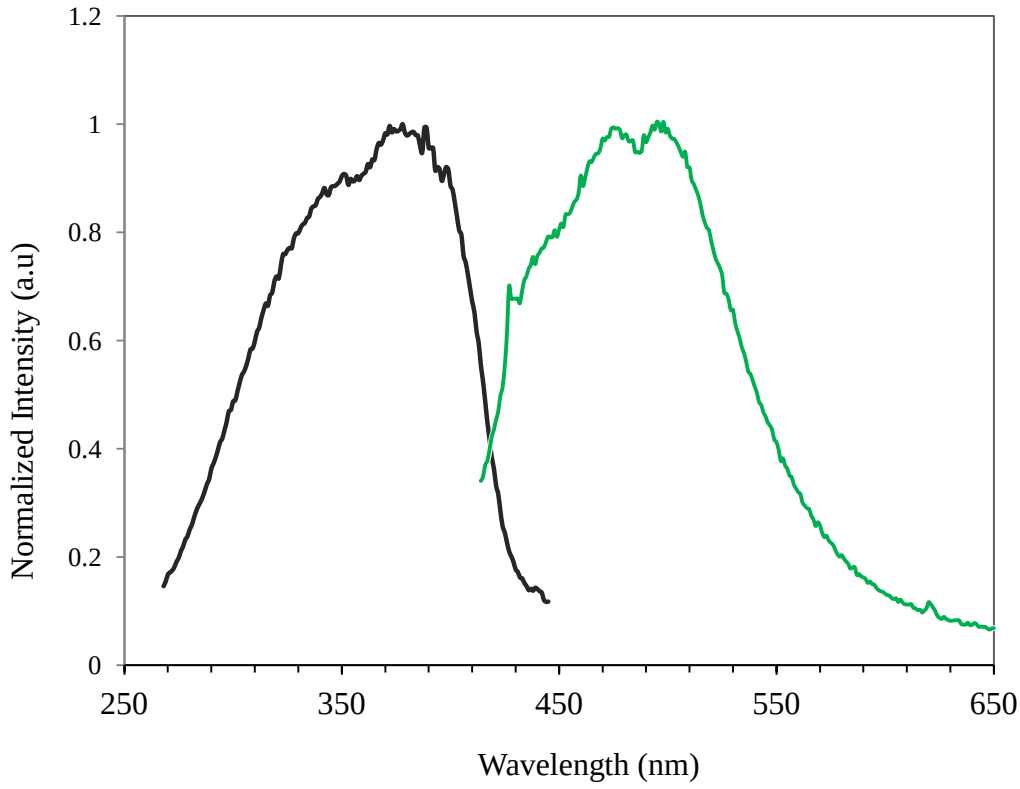

(**3**.Cd)

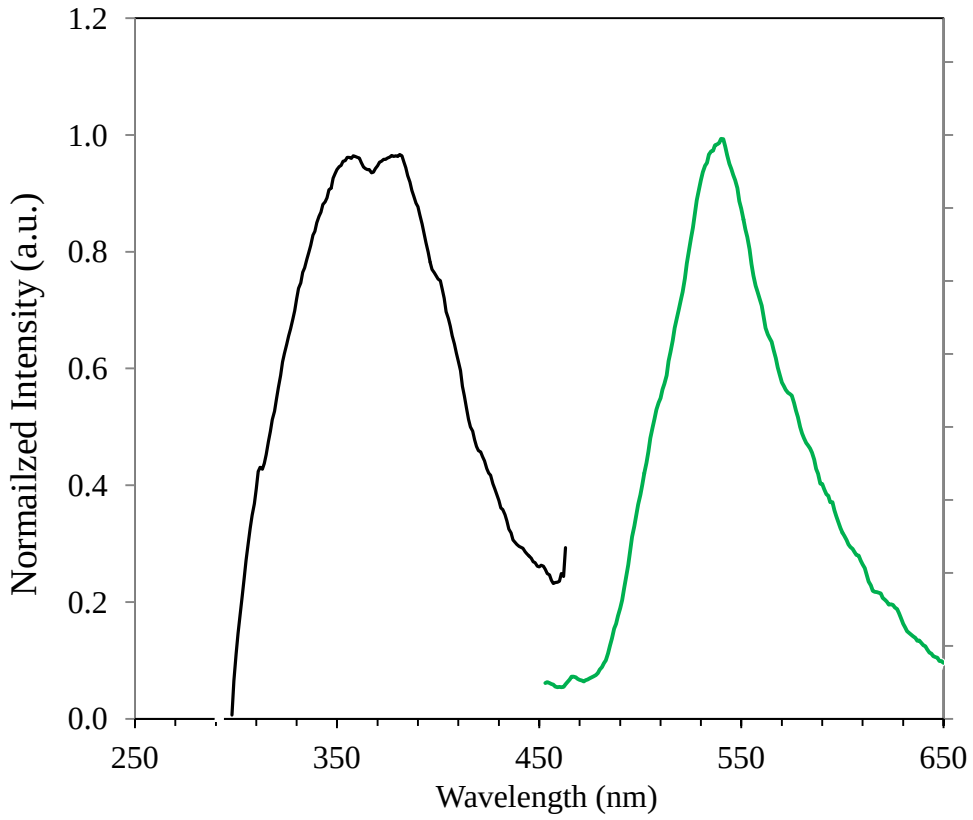

(H_2L)

Figure 3. Excitation and Emission Spectra of **1-3** and H_2L. (**1.** $\lambda_{max\ ex}$ = 382 nm**,** $\lambda_{max\ em}$ = 528 nm,); **2**. $\lambda_{max\ ex}$ = 345 nm, $\lambda_{max\ em}$ = 518 nm,); **3**. $\lambda_{max\ ex}$ = 351 nm sh, and 376 nm, $\lambda_{max\ em}$ = 448 (sh), 475 and 495 nm,); and H_2L $\lambda_{max\ ex}$ = 348 nm and 369 nm, $\lambda_{max\ em}$ = 536 nm)

Time-resolved emission measurements were used to quantify the excited-state lifetimes of new structures and to further probe the local environment of aminostilbene dicarboxylate units in **1** and **3** as compared to H_2L. The emission decay curves are shown in Figure 4. The decay curve for **1** was fitted best by a monoexponential function and shows an excited-state lifetime, τ, of 30 ps (ESI Table S2). This lifetime is relatively short and close in value to the instrument response function (IRF), and is attributed to emission from amino-stilbenoid monomeric units within the structure. Due to the ultrafast decay of **1** the results of fitting should be treated with caution, probably keeping 30 ps decay time as an upper boundary for this value. By comparison, the decay curve for H_2L (the solid ligand), was fitted best by a

biexponential function with the two decay lifetimes of τ_1 (60 ps) and τ_2 (0.25 ns) with the amplitude ratio of 17. The second and longer lived component, τ_2, is attributed to inter-chromophore coupling interactions among the amino-stilbenoid units in H_2L. For structure **3**, the decay curve was fitted best with a triexponential function, showing lifetimes, τ_1 = 0.80 ns, τ_2 = 0.13 ns and τ_3 = 2.48 ns, and relative amplitudes shown in ESI Table S2. The increase in τ_1 value for **3** over those for **1** and H_2L is consistent with the linker's more rigid configuration, stemming from the presence of the Cd-N_{amine} coordination bonds. These additional bonds could result in a larger barrier to rotation about the linker's central ethylene unit, thus minimizing energy loss to *trans-cis* isomerization. The presence of multiple lifetimes is generally attributed to complex interactions within the structure. The relatively large value of τ_3 in structure **3** and its absence from **1** and H_2L further suggests that such complex interactions among the ligand's chromophore units are more pronounced in **3**, and results from the close proximity of several of these aligned units

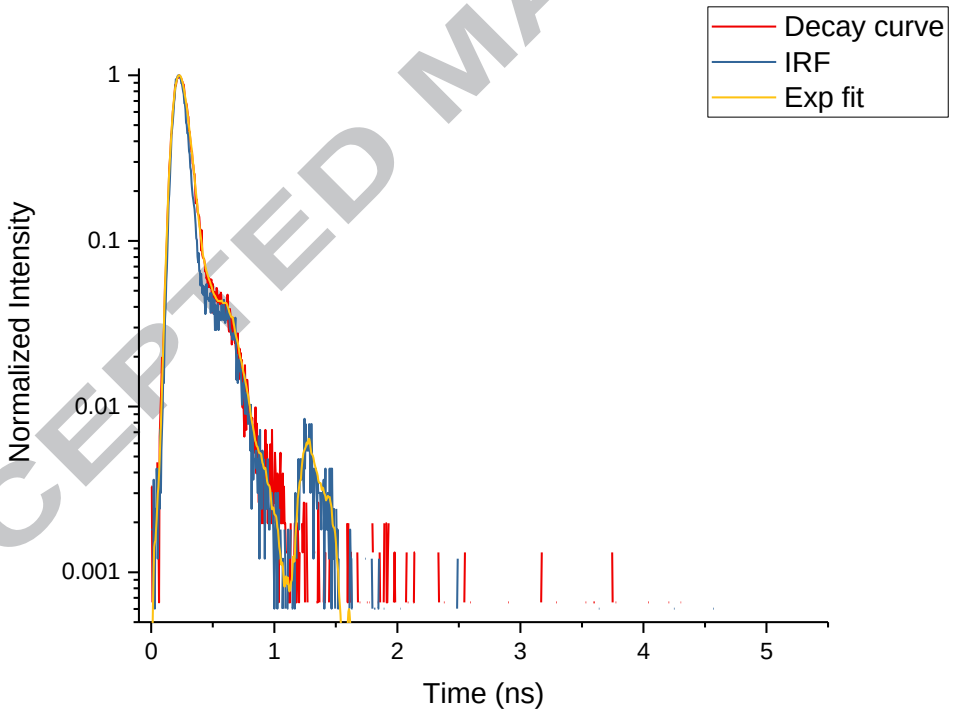

1. Yb-L

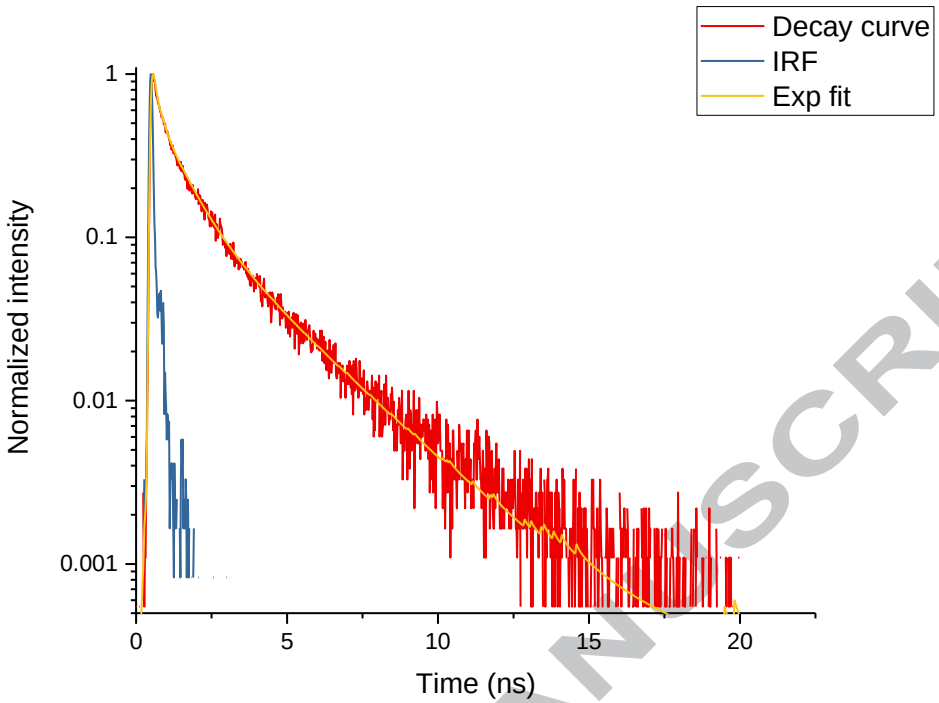

3. Cd-L

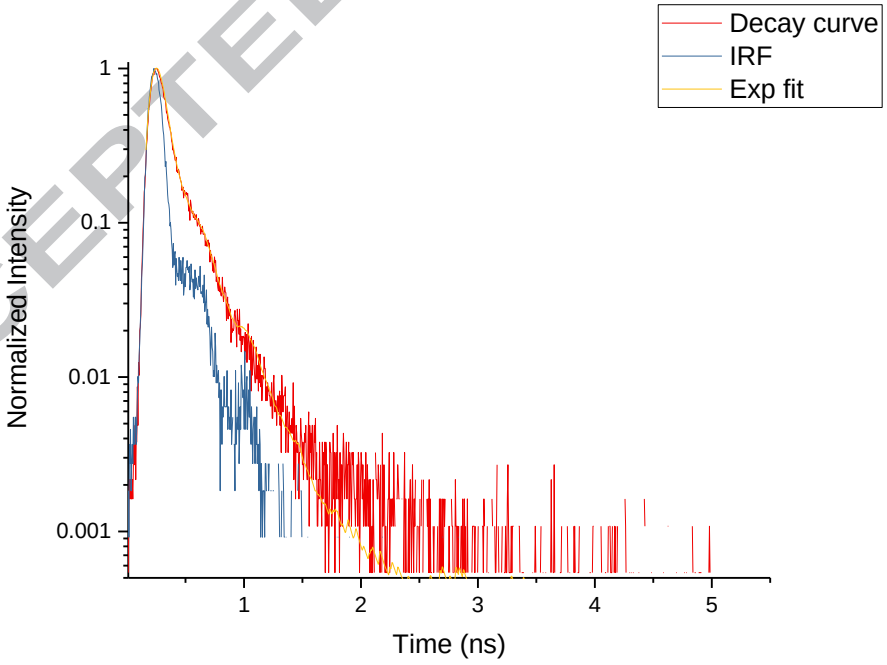

H_2L

Figure 4. Fluorescence decay curves of **1,3** and H_2L.

.

Conclusion

Two isostructural 3-D non-interpenetrating lanthanide MOFs and one Cd based coordination polymer were synthesized from the combination of 2,2'-diamino- *trans* 4,4'-stilbenedicarboxylic acid and the nitrate salts of the respective metals. The Ln-MOF structures feature large diamond shape accessible channels of dimensions 30Å x 12 Å and with the amino functional groups projecting with the channels. The cadmium based structure also crystallizes as a 1-D coordination network. The amino functional groups of the ligand are uncoordinated in the Ln-MOF structures, but coordinate the Cd atoms as Cd-$N_{(amine)}$ bonds in the cadmium based structure, thus leading to an increased rigidification of the ligand in the latter. As a result, the Cd-L structure shows fluorescence of highest intensity and longest radiative lifetime among the structures.

Conflicts of interest

There are no conflicts of interest to declare.

Acknowledgements

This work was supported by United States National Science Foundation Grants Nos. HRD-0630456, HRD-1305041, and CCHE-1213047, Department of Energy Grant No. FE0022952, and DOD Grant Nos W91INF-14-1-0084 and W911NF-15-1-0473. Electronic supporting information (ESI) available: TGA curves, FTIR spectra, PXRD patterns, and the lists of bond lengths, bond angles and other structural details are provided as ESI. Crystallographic data for the structural analysis have been deposited with the Cambridge Crystallographic Data Center as CCDC nos: 1517233, 1517234 and 1543759 for structures **1**, **2** and **3** respectively. The authors thank Professor Robert Dickson (Georgia Institute of Technology) and his students for the assistance with the luminescence lifetime measurements.

References

1 P. Deria, D. A. Gómez-Gualdrón, I Hod, R. Q. Snurr, J. T. Hupp, O. K. Farha, *J. Am. Chem. Soc.* 138 (2016) 14449.

2 Q. Yang, D. Liu, C. Zhong, J-. R. Li, *Chem. Rev.* 113 (2013) 8261.

3 D. J. Levine, T. Runčevski, M. T. Kapelewski, B. K. Keitz, J. Oktawiec, D. A. Reed, J. A. Mason, H. Z. H. Jiang, K. A. Colwell, C. M. Legendre, S. A. FitzGerald, J. R. Long, *J. Am. Chem. Soc.* 138 (2016) 10143.

4 L. E. Kreno, K. Leong, O. K. Farha, M. D. Allendorf, R. P. Van Duyne, J. T. Hupp, *Chem. Rev.* 112 *(*2012) 1105.

5 A. Schoedel, Z. Ji, O. M. Yaghi, *Nat. Energy* 1 (2016) 16034.

6 J. Cornil, D. A. dos Santos, X. Crispin, R. Silbey, J. L. Bredas *J. Am. Chem. Soc*.; 120 (1998) 1289.

7 F. Cacialli, B. S. Chauh, J. S. Kim, D. A. dos Santos, R. H. Friend, S. C. Moratti, A. B. Holmes, J. L. Bredas, *Synth Met*. 102 (1999) 924.

8 K. J. Smit, K. P. Ghiggino, *Chem. Phys. lett.* 122 **4** (1985) 369.

9 K. J. Smit, K.P. Ghiggino, *J. Photochem.* 34 **1** (1986) 23.

10 J. S.Yang, C. J. Lin, *J. Photochem. Photobio. A: Chemistry* 312 (2015) 107.

11 C. K. Lin, C. Prabhakar, J. S. Yang, *J. Phys. Chem. A* 115 (2011) 3233.

12 E. Abraham, J. Oberle, G. Jonusauskas, R. Lapouyade, C. Rulliere, *J. Photochem. Photobiol., A*, 105 (1997) 101.

13 F. D. Lewis, W. Weigel, *J. Phys. Chem. A* 104 (2000) 8146.

14 H. Goerner, H. J. Kuhn, *Adv. Photochem.*9 *(*1995) 1.

15 J. Saltiel, J. L. Charlton, Eds. *Rearrangement in Ground and Excited States*; Academic Press: New York, 1980; Vol. 3.

16 J. Saltiel, Y.-P. Sun, Eds. *Photochromism, Molecules and Systems*, Durr, H., Boaus-Laurent; H., Eds.; Elsevier: Amsterdam, 1990 p. 64 and references therein.

17 D. H. Waldeck, *Chem. Re*v. 91 **3** (1991) 415.

18 S. Hwang, J. H. Lee, C. Park, H. Lee, C. Kim, C. Park, M. H. Lee, W. Lee, J. Park, K. Kim, N.G. Park, C. Kim, *Chem. Commun*. (2007) 4887.

19 P. Senthilkumar, C. Nithya, P. Munusamy Anbarsan, *J. Mol. Model*, 19 (2013), 4561.

20 L. Wu, X. F. Zhang, Z.-Q. Li. *Inorg. Chem. Commun*. 74 (2016) 22.

21 Z. H. Xiang, C. Q. Fang, S. H. Leng, D. P. Cao, *J. Mater. Chem.*, A (2014) 7662.

22 S. S. Nagarkar, A. V. Desai, P. Samanta, S. K. Ghosh, *Dalton. Trans*. 34 (2015) 15175.

23 H. L. Jiang, D. Feng, T. F. Liu, J. R. Li, H.-C. Zhou, *J. Am. Chem.Soc*, 134 (2012), 14690.

24 A. Schaate, P. Roy, A. Godt, J. Lippke, F. Waltz, M. Wiebcke, P. Behrens, *Chem.-Eur. J.*, 17 (2011) 6643.

25 J. Tolosa, J. Bryant, K. M. Solntsev, K. Brödner, L. M. Tolbert, U. H. F. Bunz, *Chem. Eur. J.*17 (2011) 13726.

26 J. Tolosa, K. M. Solntsev, L. M. Tolbert, U. H.F. Bunz, *J. Org. Chem*. 75 (2010) 523

27 J. Saltiel, *J. Am. Chem. Soc.*, 89 **4** (1967) 1036.

28 A. Simeonov, M. Matsuishita, E. A. Juban, E. H. Thompson, J. Z. Hoffman, A. E. Beuscher, M. J. Taylor, P. Wirsching, W. Rettig, J. K. McCusker, R. C. Stevens, D. P. Millar, P. G. Schultz, R. A. Lerner, K. D. Janda, *Science*, 290 (2000) 307.

29. S. R. Mathis II, S. T. Golafale, J. Bacsa, A. Steiner, C. W. Ingram, F. P. Doty, E. Auden, K. Hattar (2017), *Dalton Trans.* 46 **2** (2017) 491.

30 C. A. Bauer, T. V. Timofeeva, T. B. Settersten, B. D. Patterson, V.H. Liu, B. A. Simmons, M. D. Allendorf, *J. Am. Chem. Soc*. 129 (2007) 7136.

31 C. A. Bauer, S. C. Jones, T. L. Kinnibrugh, P. Tongwa, R. A. Farrell, A. Vakil, T. Timofeeva, V. Khrustalev, M. D. Allendorf, *Dalton Trans.* 43 (2014**)** 2925.

32 X. L. Wang, C. Qin, E. B. Wang, L. Xu, *Cryst. Growth Des*., 6 (2006) 2061.

33 K. L. Huang, Y. T. Hei, M. Huang, *J. Coor. Chem*. 61 (2008) 2735.

34 J. Yang, J. F. Ma, S. R. Batten, Z. M. Su. *Chem. Commun*, (2008) 2233.

35 H. Y. Wang, S. Gao, L. H. Huo, S. W. Ng, J. G. Zhao, *Cryst. Growth. Des*., 8 (2008) 665.

36 Y. Ma, A. L. Cheng, J. Y. Zhang, Q. Yue, E. Q. Zhao, *Cryst. Growth. Des*., 9 (2009) 867.

37 D. H. Lee, and G. Park, *Acta. Cryst. E.* 64 (2008) M861.

38 G. Park, H. Kim, G. H. Lee, S. K. Park, K. Kim, *Bull. Korean Chem. Soc*., 27 (2006) 443.

39 J. Yang, J. F. Ma, Y. Y. Liu, S. R. Batten, *CrystEngComm,* 11 (2009) 151.

40 L. Zhang, Y. L. Yao, Y. X. Che, and J. M. Zheng, *Cryst. Growth. Des*. 10 (2010) 528.

41 J. Liu, Y. Wang, *J. Chem. Crystallography.* 41 (2011) 1940.

42 H-. Y. Wang, S. Gao, J.-G., Zhao, S. W. Ng. *Acta. Cryst E* 62 (2006) M3127.

43 X. L. Wang, Y. Q. Chen, Q. Gao, H. Y. Lin, G. C. Liu, J. X. Zhang, A. X. Tian, *Cryst. Growth. Des*. 10 (2010) 2174.

44 X. L. Wang, Z. C. Guo, G. C. Liu, Y. Qu, S. Yang, H. Y. Lin, J. W. Zhang, *CrystEngCommun*. 15 (2013) 551.

45 A. L. Cheng, N. Liu, Y. F. Yue, Y.W. Jiang, E. Q. Gao, C. H. Yan, M. Y. He, *Chem. Commun*. (2007) 407.

46 C. A. Bauer, T. V. Timofeeva, T. B. Settersten, B. D. Patterson, V. H. Liu, B. A. Simmons, M. D. Allendorf, *J. Am. Chem. Soc*. 129 (2007) 7136.

47 A. L. Cheng, Y. Ma, J. Y., Zhang, E. Q. Gao, *Dalton Trans.* (2008) 1993.

48 K. L. Huang, X. Liu, G. M. Liang, *Inorg. Chim. Acta*, 362 (2009) 1565.

49 A. L. Cheng, Y. Ma, Q. A. Sun, E. Q. Gao, *CrystEngComm.*, 13 (2011*)* 2721.

50 A. Naeem, V. P. Ting, U. Hintermair, M. Tian, R. Telford, S. Halim, H. Nowell, M. Hołyńska, S. J. Teat, I. J. Scowen, S. Nayak, *Chem. Commun.* 52 (2016) 7826.

51 J. Zhang, S. Yao, S. Liu, B. Liu, X. Sun, B. Zheng, G. Li, Yi Li , Q. Huo, Y. Liu, *Cryst. Growth Des.* 17 (2017) 2131.

52 Z. Deng, L. Huo, H. Wang, S. Gao, H. Zhao, *CrystEngComm.* 12 (2010) 1526.

53 Y. Li, D. Song, *Cryst. Eng. Comm.* 13 (2011) 1821.

54 Z. P. Deng, L. H. Huo, H. Y. Wang, S. Gao, H. Zhao, *CrystEngComm* 12 (2010*)* 1526.

55 Rigaku Oxford Diffraction, (2015).

56 O. V. Dolomanov, L. J. Bourhis, R. J. Gildea, J. A. K Howard, H. J. Puschmann, *Appl. Cryst.* 42 (2009) 339.

57 G..M. Sheldrick, *Acta Cryst C* 71 ,**1**, (2015) 3.

58 G. M. Sheldrick, *Acta Cryst*. A 64 (2008) 339.

59. *APEX2*, Bruker AXS Inc., Madison, Wisconsin, USA, Bruker (2016).

60 S. Hausdorf, F. Baitalow, J. Seidel, F. O. R. L Mertens, *J. Phys. Chem*. A. 111, (2007), 4259.

61 V. A. Blatov, A. P. Shevchenko, D. M. Proserpio, *Cryst. Growth Des.* 14, (2014), 3576.

62 J.-Li. Zhu, G. –Q. Jiang, X.-Q. Guo,[b] Y.-F. Tang, M. Wang, *Acta Cryst. E* 71, **9** (2015) 1022.

63 F. D. Lewis , S. R. Kalgutkar, J.-S. Yang, *J. Am. Chem. Soc.*, 121 **51** (1999) 12045.

64 A. Kawski, A. Kubicki, B. Kuklinski, T. Z. Nowosielski, *Naturforsch*, 51A (1996) 1153.

65 J. Cornil, D. A. dos Santos, X. Crispin, R. Silbey, J. L. Bredas, *J. Am. Chem. Soc.* 120 *(*1998) 1289.

66 L. Zhenda, L. Wen, Z. Ni, Y. Li, H. Zhu, Q. Meng, *Cryst. Growth Des. 7 2 (*2007*)* 268.

67 L. D. Rocha, F. A. Carlos, A. Paz, Almeida, D. Ananias, *Chem. Soc. Rev*., 40 (2011) 926.

68 M. D. Allendorf, C. A. Bauer, R. K. Bhakta, R. J. T. Houk, *Chem. Soc. Rev*., 38 (2009)1330.

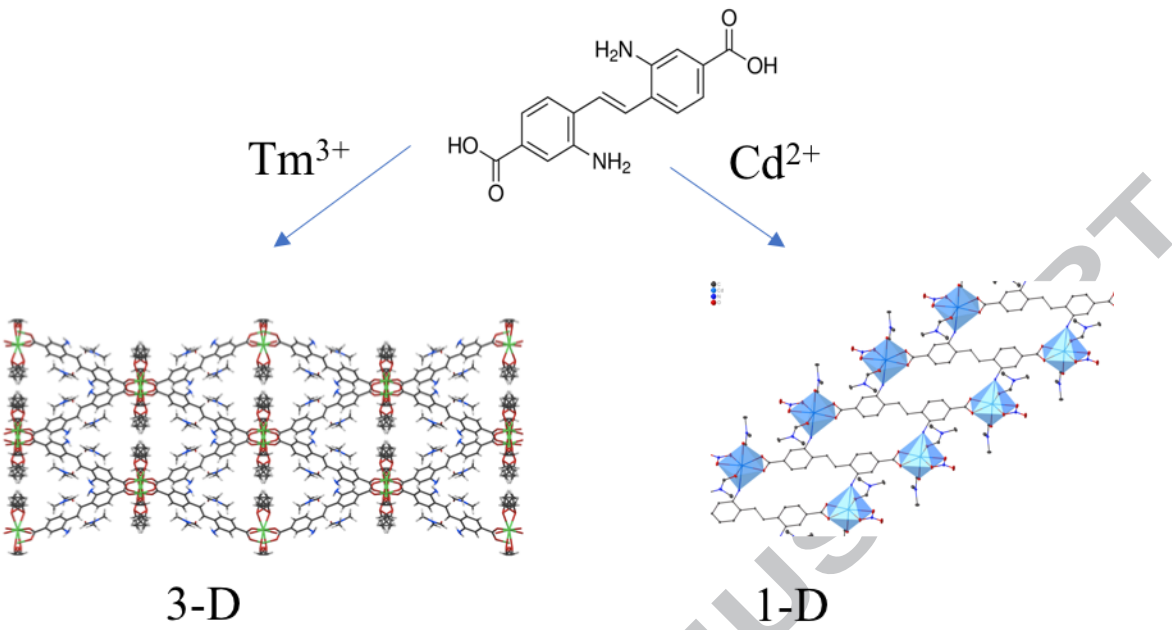

3-D open lanthanide metal organic framework and 1-D cadmium coordination polymer from the combination of 2,2'-diamino-*trans* 4,4'-stilbenedicarboxylic acid with the respective metal ion.

- Diaminostilbene dicarboxylic acid produces open framework 3-D MOFs with lanthanide ions and 1-D open coordination polymer with cadmium ions.
- The structures show ligand based fluorescence when excited by UV radiation, with the Cd structure showing the brightest emission and longest radiative lifetime.